Plasticity is Friction: Towards Controlling Deformables with Contact-Implicit MPC

Bibit Bianchini and Michael Posa

***Abstract*— We mathematically formulate plasticity identically to frictional stick-slip transitions, enabling use of contact-implicit model-based control techniques that optimize for contact mode sequences in real time to manipulate elastoplastic deformable materials.**

I. Introduction

We present a new insight that can enable manipulating elastoplastic deformables with contact-implicit model predictive control (CI-MPC) techniques: plastic deformation can be seen as analogous to (and modeled identically to) frictional stick-slip transitions. Plastic yield occurs when an internal stress reaches the material's yield stress. This can be modeled as a stick-slip transition where the "normal force" is fixed such that the "tangential force" that transitions from sticking to sliding instead represents transitioning from no deformation to plastic yield. When combined with smooth force elements (springs) in different configurations, this "plastic" joint enables modeling nodal networks that can represent 3D elastic, plastic, and elastoplastic materials with different properties. This modeling choice fits seamlessly into recent CI-MPC approaches that optimize for state, input, and contact mode sequences, where now contact modes can indicate when plastic deformation occurs. In this work, we:

- Describe the complementarity-based formulation of rigid body contact dynamics (§III);
- Introduce our new insight on plasticity as a frictional stick-slip transition, which can be expressed in the same complementarity form as rigid body dynamics (§IV);
- Present how using plastic elements modeled with our hybrid dynamics can achieve similar phenomena to real elastoplastic materials, including elastic regions, permanent plastic strain, and even strain hardening (§IV); and
- Motivate and propose our ongoing work that leverages this representation for manipulating deformable bodies with CI-MPC (§V, §VI).

A. Notation

a) Non-contact related: State $x \in \mathbb{R}^{n_x}$ comprises configuration $q \in \mathbb{R}^{n_q}$ and velocity $v \in \mathbb{R}^{n_v}$; inputs $u \in \mathbb{R}^{n_u}$ map to generalized coordinates via $P \in \mathbb{R}^{n_v \times n_u}$. Other terms: $M \in \mathbb{R}^{n_v \times n_v}$ mass matrix, $k \in \mathbb{R}^{n_v}$ continuous generalized forces, Δt time discretization. For conciseness, if time step subscripts are omitted, we use the superscript $'$ to denote the next time step (e.g. $\{x_k, x_{k+1}\} = \{x, x'\}$).

*This work was supported by the RAI Institute and the National Science Foundation under Grant No. FRR-2238480.

Bibit Bianchini and Michael Posa are with the Department of Mechanical Engineering and Applied Mechanics, University of Pennsylvania, Philadelphia, PA 19104, USA {bibit,posa}@seas.upenn.edu

b) For external rigid-body contacts (§III): The complementarity variable $\lambda \in \mathbb{R}^{n_\lambda} = \mathbb{R}^{(2+n_f)n_c}$ (for n_c as number of contacts and n_f as number of friction directions used for approximating the friction cone as a polyhedron) comprises a vector of normal forces $\lambda_n \in \mathbb{R}^{n_c}$, a vector of tangential forces $\lambda_t \in \mathbb{R}^{n_c n_f}$, and a vector of slack variables $\zeta \in \mathbb{R}^{n_c}$ usually equal to the magnitude of the contacts' relative sliding speeds (see [1]). Other rigid-body contact terms: $J_n \in \mathbb{R}^{n_v \times n_c}$ and $J_t \in \mathbb{R}^{n_v \times n_c n_f}$ respective normal and tangential contact Jacobians, $\tilde{\mu} \in \mathbb{R}^{n_c \times n_c}$ diagonal matrix of friction coefficients per contact pair, $E \in \mathbb{R}^{n_c n_f \times n_c}$ matrix of ones and zeros (see [1]), and $\phi \in \mathbb{R}^{n_c}$ signed distances.

c) For internal plastic forces (§IV): Subscripts p denote "plastic" and thus represent the internal force equivalent of external force terms (e.g. n_{pc} is the number of internal plastic connections). While external contacts have normal J_n and tangential J_t contact Jacobians, internal contacts only need the tangential analog, so we call this J_p instead of J_{pt}. Internal contacts have complementarity variables $[\sigma; \gamma]$ where σ is the analog to λ_t, γ is the analog to ζ, and there is no analog to λ_n (which can be considered fixed).

II. Prior Work

A. Deformable Manipulation

Deformable object manipulation is a longstanding challenge in robotics. The high dimensionality of deformable bodies complicates state representation, state estimation, and dynamics predictions. Recent surveys [2], [3] acknowledge progress in manipulating 1D (e.g. rope) and 2D (e.g. fabric) deformables, and of linear elastic materials in particular. Plastic deformation introduces hybrid dynamics, which complicates control strategies similarly to the challenges of contact-driven hybrid dynamics [4], [5]. This presents a challenge and suggests a solution: we can take inspiration from how the contact-implicit control community handles the hybrid nature of contact, and apply those same insights into the hybrid nature of plasticity.

B. CI-MPC

Recent progress in contact-implicit control has enabled real-time performance for many contact-rich tasks. One approach uses local complementarity-based dynamics approximations [6], [7], encouraging consensus between local non-smooth rigid-body contact constraints and local dynamics, while exploring contact modes via small-scale mixed integer optimization. Recent speed improvements to

the local CI-MPC algorithm [8] in combination with low-dimensional, global sampling [9] enables generalizable performance across a high number of modeled contacts. Other distinct but similar approaches use artificially smoothed contact dynamics, allowing online gradient-based algorithms to explore different contact modes [10]–[13].

III. Background in Modeling External Rigid-Body Contacts

A discrete-time dynamics function can be written as

$$x' = f(x, u), \tag{1}$$

where f can encode any nonlinear or non-smooth phenomena. Particularly for contact-rich systems, this f is hybrid and, as a result, highly nonlinear in state and input.

Without making any approximations yet, it can often be useful to replace f with a new function that takes an additional input argument: contact forces. The dynamics of a contact-rich system can be generally written as

$$x' = g\left(x, u, \lambda\right), \tag{2a}$$
$$0 \leq \lambda \perp \pi\left(x, u, \lambda\right) \geq 0, \tag{2b}$$

where the dynamics g depend on contact forces/impulses λ, which are the solution to a nonlinear complementarity problem (NCP) [14] in (2b). The NCP elegantly embeds the multi-modal nature of contact-rich systems. If π is linear in x, u, λ, then the NCP becomes a linear complementarity problem (LCP).

Works from the 1990s showed how to formulate rigid body dynamics in the form of an LCP. While there are many formulations that do so with slight variations, here we will review the variation from [1], as it is cleanly adapted for our later proposed plasticity representation.

For a system with possibly multiple contacts between any two rigid bodies, [1] expresses rigid body dynamics via the force update equation and a backwards Euler step,

$$v' = v + M^{-1}\left(J_n\lambda_n + J_t\lambda_t + \Delta t(k + Pu)\right), \tag{3a}$$
$$q' = q + \Delta t v', \tag{3b}$$

where complementarity variables are found by solving an LCP of the form $0 \leq \lambda \perp J\lambda + b \geq 0$ where

$$\lambda = \begin{bmatrix} \lambda_t \\ \lambda_n \\ \zeta \end{bmatrix}, \tag{4a}$$
$$J = \begin{bmatrix} J_t^T M^{-1} J_t & J_t^T M^{-1} J_n & E \\ J_n^T M^{-1} J_t & J_n^T M^{-1} J_n & 0 \\ -E^T & \tilde{\mu} & 0 \end{bmatrix}, \tag{4b}$$
$$b = \begin{bmatrix} J_t^T\left(v + \Delta t M^{-1}(k + Pu)\right) \\ \frac{1}{\Delta t}\phi(q) + J_n^T\left(v + \Delta t M^{-1}(k + Pu)\right) \\ 0 \end{bmatrix}. \tag{4c}$$

The interpretation of the three rows is as follows:

a) Row 1: $0 \leq \lambda_t \perp E\zeta + J_t^T v' \geq 0$. Friction force opposes direction of relative motion. ζ is constrained be at least the magnitude of the relative contact velocity.

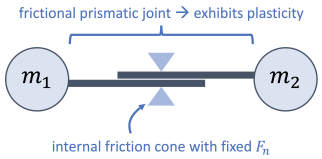

Fig. 1. Two particles connected via a plastic joint. Think of the two arms as frictional and held together with fixed clamping force F_n; the arms slide relative to each other when the tangential force overcomes μF_n.

b) Row 2: $0 \leq \lambda_n \perp \phi' \geq 0$. No contact forces at a distance. There can be no penetration at the next timestep.

c) Row 3: $0 \leq \zeta \perp \tilde{\mu}\lambda_n - E^T\lambda_t \geq 0$. If sliding, contact force is on the surface of friction cone. Friction must stay on or within the friction cone.

IV. Representing Elastoplasticity with Internal Frictional Forces

Prior works have formulated plasticity as an LCP, with some dating in the 1980s [15] and the first claiming to handle dynamic cases much more recently in 2019 [16]. Applications have been limited to static geotechnical problems [17] and 2D toy problems [16]. To the best of our knowledge, plasticity as an LCP has not been used in the field of robotics.

A. Introducing Plastic Joints

Consider a simple deformable body modeled as two point masses connected by a frictional slider (Fig. 1). This frictional slider can be considered a prismatic joint between the two masses, where the joint itself has stiction (i.e. a yield force) that needs to be overcome before motion is permitted. For this 1D plastic slider (which can exist in 1D, 2D, or 3D space), the number of tangential force directions $n_{pf} = 2$, corresponding to positive and negative displacements along the 1D direction of travel. The following relationships to rigid-body LCP dynamics describe this plastic joint's motion:

a) Analog to Row 1: $0 \leq \sigma \perp E_p\gamma + J_p^T v' \geq 0$. Internal plastic resistance force opposes the direction of relative motion. γ must be at least the relative contact speed (in Fig. 2 for the plastic joint, this would be $\dot{d}$).

b) Analog to Row 2: There is no equivalent signed distance / contact force complementarity, since the signed distance is always zero and the "normal force" can be considered fixed (at f_{yield}/μ_p).

c) Analog to Row 3: $0 \leq \gamma \perp \Delta t f_{\text{yield}} - E_p^T\sigma \geq 0$. If plastically deforming, the internal plastic resistance is equal to the joint's yield force. The internal plastic resistance is upper bounded by the yield force.

Thus, an LCP of the form $0 \leq \lambda \perp J\lambda + b \geq 0$ can describe a system with only internal plastic joints (and no external contact pairs) with

$$\lambda = \begin{bmatrix} \sigma \\ \gamma \end{bmatrix}, \tag{5a}$$
$$J = \begin{bmatrix} J_p^T M^{-1} J_p & E_p \\ -E_p^T & 0 \end{bmatrix}, \tag{5b}$$
$$b = \begin{bmatrix} J_p^T\left(v + \Delta t M^{-1}(k + u)\right) \\ \Delta t f_{\text{yield}} \end{bmatrix}. \tag{5c}$$

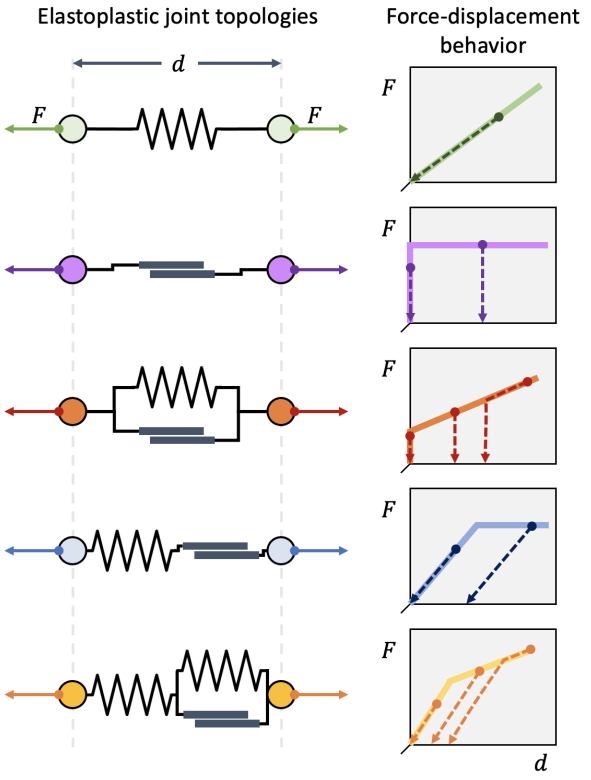

Fig. 2. Different elastoplastic behaviors can be achieved via different topological combinations of springs (for elasticity) and frictional prismatic joints (for plasticity). The dots and dashed lines on the force-displacement curves indicate the unloading behavior from a reached operating point. Any dashed lines that do not return to the origin exhibit a leftover plastic deformation.

For a system with both external contacts and internal plastic joints, the LCP variables λ and vector b can be stacked as $[\lambda_{\text{ext}}; \lambda_{\text{int}}] = [\lambda_t; \lambda_n; \zeta; \sigma; \gamma]$ and $[b_{\text{ext}}; b_{\text{int}}]$, respectively. The matrix J contains off-diagonal coupling blocks, i.e.

$$J = \begin{bmatrix} J_{\text{ext}} & J_{\text{coupling}} \\ J_{\text{coupling}}^T & J_{\text{int}} \end{bmatrix}, \quad J_{\text{coupling}} = \begin{bmatrix} J_t^T M^{-1} J_p & 0 \\ J_n^T M^{-1} J_p & 0 \\ 0 & 0 \end{bmatrix}. \tag{6}$$

B. Topologies for Elastoplasticity

The introduction of internal plastic contacts can be applied to many different topological configurations to achieve a desired elastoplastic behavior. Generally, frictional sliders achieve plastic deformation, and springs achieve elastic deformation. Their combinations can produce different characteristic force-displacement curves, as depicted in Fig. 2.

For topologies with a spring and plastic slider in series (i.e. the bottom two examples in Fig. 2), the relative sliding speed of the plastic slider is not $\dot{d}$ and depends on the node location between the spring and slider. We can represent this by increasing the state dimension by 1 per elastoplastic joint denoting this intermediate node location; its derivative can be approximated based on the forward projected node location compared to its current value.

C. Modeling Deformables as Mass Networks with Elastoplastic Connections

These 1D elastoplastic joints can be constructed in series to model deformable linear objects (DLOs) [18], in a 2D triangulated network to model deformable surfaces e.g. cloth, or in a tetrahedral network to model deformable volumes.

Consider a 3D deformable body. Modeling this body as a 3D tetrahedral network of points connected via elastoplastic joints can:

- Approximately capture a desired Young's modulus, by properly setting spring constants of each joint. A method for determining spring constants given a network structure and a desired Young's modulus was first shown in [19] with a more thorough derivation for the 3D case in [20].
- Approximately capture a desired yield stress, by properly setting stick-slip transition forces of each plastic joint. We propose in this work that a slight tweak on the same approach used for spring constants can be used for setting stick-slip transition forces of the plastic frictional slider.
- Approximately capture a fixed Poisson ratio, as a property of the network structure itself. E.g. [20] shows $\nu = \frac{1}{3}$ for a 2D deformable surface modeled with a network of equilateral triangles and $\nu = \frac{1}{4}$ for a 3D deformable volume modeled with a network of regular tetrahedra.

To determine the yield force for an elastoplastic joint such that the network approximately has the yield stress of the desired 3D material, we use the following mechanical properties. Yield stress and Young's modulus are related by

$$\sigma_{\text{yield}} = E\epsilon_{\text{yield}}, \qquad \text{where } \epsilon_{\text{yield}} := \frac{\Delta l_{\text{yield}}}{l}, \tag{7}$$

for a Young's modulus E and yield strain ϵ_{yield} defined by the ratio of yield displacement Δl_{yield} to the undeformed length l. When a spring is in series with a plastic frictional joint to model an elastoplastic material, the force through the spring is equivalent to the force through the frictional joint, including at yield,

$$f_{\text{yield}} = k_{\text{spring}} \Delta l_{\text{yield}} = \frac{k_{\text{spring}} l \sigma_{\text{yield}}}{E}. \tag{8}$$

This means given an arbitrary tetrahedral network structure that aims to approximate a 3D material's Young's modulus and yield stress, we:

1) Solve for each elastoplastic connection's spring constant according to [19], [20].
2) Solve for each elastoplastic connection's yield force according to (8), using the computed spring constant.

V. Background in LCS-Based CI-MPC

With a mathematical formulation of elastoplastic materials that fits the same LCP-based framework that represents frictional contact, the same CI-MPC techniques that optimize over sequences of external contact modes can now also optimize over sequences of internal plastic deformation modes.

A. Nonlinear Optimal Control Formulation

We are interested in solving the nonlinear MPC problem for systems with state x and inputs u,

$$\min_{x_k,u_k} \sum_{k=0}^{N-1} (x_k^T Q_k x_k + u_k^T R_k u_k) + x_N^T Q_N x_N \tag{9a}$$

$$\text{s.t.} \quad x_{k+1} = f(x_k, u_k), \tag{9b}$$

$$x_0 = x_{\text{init}}, \tag{9c}$$

$$(x_k, u_k) \in \mathcal{C}, \tag{9d}$$

$$\text{for } k \in \{0, \dots, N\}. \tag{9e}$$

This optimization problem finds the dynamically feasible state and input sequence that minimizes state- and input-based costs. The sequences must be compatible with the generic dynamics function f in (9b), which is not generally feasible in real time when f embeds contact-rich dynamics.

B. LCS Dynamics

To make the optimization problem (9) more tractable, the dynamics f need to be approximated, but in a way that maintains the important features of contact. One option is to linearize the dynamics function g and complementarity vector function π from (2) with respect to x, u, λ. The result is called a linear complementarity system (LCS) [21]. An LCS describes the state and contact force trajectories for an input sequence starting from x_0 such that

$$x_{k+1} = Ax_k + Bu_k + D\lambda_k + d, \tag{10a}$$

$$0 \leq \lambda_k \perp Ex_k + F\lambda_k + Hu_k + c \geq 0. \tag{10b}$$

C. CI-MPC with LCS Dynamics

LCS dynamics are the backbone of the line of CI-MPC controllers called Consensus Complementarity Control (C3) [7] with many subsequent works [6], [8], [9]. C3 poses the control problem with the dynamics expressed as an LCS (substituting (10) for (9b)) using x_{init} (and some nominal u_0, λ_0) as the LCS linearization point.

While this is still computationally intensive in practice because of the complementarity constraint (10b), C3 converges to the solution of this optimization problem using the alternating direction of multipliers (ADMM) to iteratively solve the optimization problem while satisfying certain constraints at a time. In practice, it is more useful to terminate C3 early after a few ADMM iterations. Using a suboptimal solution at a faster rate is more performant than a more optimal solution at a slower rate.

VI. Controlling Deformables with CI-MPC

The optimization problem solved by C3 is valid for any system with LCS dynamics. While all previous demonstrations of C3 have shown rigid body manipulation, we seek to apply this control paradigm to deformable systems using our LCP-based plasticity formulation. Progress in this aim is preliminary, so this section provides ongoing work and thoughts on how different aspects of a hardware demo of manipulating dough have been and will be addressed.

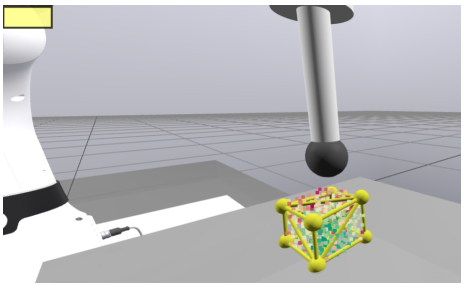

Fig. 3. We use an extension of Drake with MPM deformable dynamics [22] to simulate a block of dough (red and green points), which we manipulate with a Franka arm equipped with a spherical end effector. Our controller operates on LCS dynamics with the dough represented as a sparse set of 8 vertices connected with 18 elastoplastic joints (yellow spheres and lines). The vertex locations update in response to the current state of the MPM points by taking the location of the extreme MPM points in the 8 $[\pm 1, \pm 1, \pm 1]$ directions.

A. Representing a Deformable for Control

We represent a volume of dough as a set of coarse, connected tetrahedra whose vertex locations encode the configuration of the deformable. We are confident that our controller can handle reasonably interesting 3D dough shapes: the rate of the C3 controller degrades with higher $n_x + n_u + n_\lambda$ (among other terms). Push Anything [8] showed impressive scaling of these numbers was possible with C3+: $58+3+76 = 137$. In our preliminary demo (depicted in Fig. 3) where the deformable is modeled by 8 vertices connected by 18 elastoplastic joints (without intermediate nodes) and manipulated by a 3-DoF end effector, $n_x + n_u + n_{\lambda,\text{external}} + n_{\lambda,\text{internal}} = 54 + 3 + 36 + 36 = 129$. This gives us room to match Push Anything control rates easily, with potential to scale to more vertices by trading off with other parameters that affect control rate (e.g. MPC horizon, ADMM iterations, number of end effector samples [9]).

B. Simulation

For initial validation, we test our controller in simulation (Fig. 3). Many robotics simulators handle deformables [23]–[25], but not many model plasticity. Of those that offer elastoplastics [26]–[29], a GPU-accelerated extension [22] of Drake that implements the material point method (MPM) [30] was – albeit only 10% real time – the fastest elastoplastic simulator we tested for our use. This simulation is acceptable for validation (since we can slow down our control loop rate to emulate real-time deployment) and is unused for hardware.

C. Hardware Challenges

The main challenge for hardware deployment is real-time deformable state estimation. Achieving real-time rates for 3D deformable object tracking has been a goal for decades [31], [32]. Current trackers that claim real-time deformable state estimation have limitations such as only producing bounding boxes [33], tracking only DLOs (1D) [18], [34], requiring idealistic minimal occlusion [35], [36], and/or requiring substantial textural cues [37]. It is unclear which – if any of these existing solutions – will be the most robust, or if a custom approach will be necessary for our use case.

REFERENCES

[1] D. E. Stewart and J. C. Trinkle, "An implicit time-stepping scheme for rigid body dynamics with inelastic collisions and coulomb friction," *International Journal for Numerical Methods in Engineering*, vol. 39, no. 15, pp. 2673–2691, 1996.

[2] L. Han and H. Wang, "Robotic manipulation of deformable objects: a comprehensive review," *Robotic Intelligence and Automation*, pp. 1–16, 2026.

[3] F. Gu, Y. Zhou, Z. Wang, S. Jiang, and B. He, "A survey on robotic manipulation of deformable objects: Recent advances, open challenges and new frontiers," *arXiv preprint arXiv:2312.10419*, 2023.

[4] S. A. Khader, H. Yin, P. Falco, and D. Kragic, "Data-efficient model learning and prediction for contact-rich manipulation tasks," *IEEE Robotics and Automation Letters*, vol. 5, no. 3, pp. 4321–4328, 2020.

[5] S. Kolev and E. Todorov, "Physically consistent state estimation and system identification for contacts," in *2015 IEEE-RAS 15th International Conference on Humanoid Robots (Humanoids)*. IEEE, 2015, pp. 1036–1043.

[6] W. Yang and M. Posa, "Dynamic on-palm manipulation via controlled sliding," in *Robotics: Science and Systems (RSS)*, Jul. 2024. [Online]. Available: https://roboticsconference.org/program/papers/12/

[7] A. Aydinoglu, A. Wei, W.-C. Huang, and M. Posa, "Consensus complementarity control for multi-contact mpc," *IEEE Transactions on Robotics*, 2024.

[8] H. Bui, Y. Gao, H. Yang, E. Cui, S. Mody, B. Acosta, T. S. Felix, B. Bianchini, and M. Posa, "Push anything: Single- and multi-object pushing from first sight with contact-implicit mpc," in *To appear in the IEEE International Conference on Robotics and Automation (ICRA)*, 2026.

[9] S. Venkatesh, B. Bianchini, A. Aydinoglu, W. Yang, and M. Posa, "Approximating global contact-implicit mpc via sampling and local complementarity," *IEEE Robotics and Automation Letters (RA-L)*, vol. 10, no. 11, pp. 12 117–12 124, 2025. [Online]. Available: https://ieeexplore.ieee.org/document/11181073

[10] G. Kim, D. Kang, J.-H. Kim, S. Hong, and H.-W. Park, "Contact-implicit mpc: Controlling diverse quadruped motions without pre-planned contact modes or trajectories," *arXiv preprint arXiv:2312.08961*, 2023.

[11] S. L. Cleac'h, T. Howell, M. Schwager, and Z. Manchester, "Fast contact-implicit model-predictive control," *arXiv preprint arXiv:2107.05616*, 2021.

[12] V. Kurtz, A. Castro, A. Ö. Önol, and H. Lin, "Inverse dynamics trajectory optimization for contact-implicit model predictive control," *arXiv preprint arXiv:2309.01813*, 2023.

[13] Y. Tassa, T. Erez, and E. Todorov, "Synthesis and stabilization of complex behaviors through online trajectory optimization," in *2012 IEEE/RSJ International Conference on Intelligent Robots and Systems*. IEEE, 2012, pp. 4906–4913.

[14] D. E. Stewart, *Dynamics with Inequalities: impacts and hard constraints*. SIAM, 2011.

[15] G. Maier and G. Novati, "Elastic-plastic boundary element analysis as a linear complementarity problem," *Applied Mathematical Modelling*, vol. 7, no. 2, pp. 74–82, 1983.

[16] D. Rodigari, A. Franchi, F. Genna, P. Crespi, and R. De Col, "A linear complementarity approach to the time integration of dynamic elastic–plastic structural problems," *Meccanica*, vol. 54, no. 10, pp. 1597–1609, 2019.

[17] R. Zhao, C. Li, L. Zhou, and H. Zheng, "A sequential linear complementarity problem for multisurface plasticity," *Applied Mathematical Modelling*, vol. 103, pp. 557–579, 2022.

[18] S. Javdani, S. Tandon, J. Tang, J. F. O'Brien, and P. Abbeel, "Modeling and perception of deformable one-dimensional objects," in *2011 IEEE international conference on robotics and automation*. IEEE, 2011, pp. 1607–1614.

[19] A. V. Gelder, "Approximate simulation of elastic membranes by triangulated spring meshes," *Journal of graphics tools*, vol. 3, no. 2, pp. 21–41, 1998.

[20] B. Lloyd, G. Székely, and M. Harders, "Identification of spring parameters for deformable object simulation," *IEEE transactions on visualization and computer graphics*, vol. 13, no. 5, pp. 1081–1094, 2007.

[21] W. Heemels, J. M. Schumacher, and S. Weiland, "Linear complementarity systems," *SIAM journal on applied mathematics*, vol. 60, no. 4, pp. 1234–1269, 2000.

[22] C. Yu, W. Du, Z. Zong, A. Castro, C. Jiang, and X. Han, "A Convex Formulation of Material Points and Rigid Bodies with GPU-Accelerated Async-Coupling for Interactive Simulation," Jul. 2025, arXiv:2503.05046 [cs]. [Online]. Available: http://arxiv.org/abs/2503.05046

[23] E. Todorov, T. Erez, and Y. Tassa, "Mujoco: A physics engine for model-based control," in *2012 IEEE/RSJ International Conference on Intelligent Robots and Systems*. IEEE, 2012, pp. 5026–5033.

[24] NVIDIA, "Isaac Sim." [Online]. Available: https://github.com/isaac-sim/IsaacSim

[25] M. Macklin, "Warp: A high-performance python framework for gpu simulation and graphics," https://github.com/nvidia/warp, March 2022, nVIDIA GPU Technology Conference (GTC).

[26] Genesis Authors, "Genesis: A generative and universal physics engine for robotics and beyond," December 2024. [Online]. Available: https://github.com/Genesis-Embodied-AI/Genesis

[27] Z. Huang, Y. Hu, T. Du, S. Zhou, H. Su, J. B. Tenenbaum, and C. Gan, "PlasticineLab: A Soft-Body Manipulation Benchmark with Differentiable Physics," Apr. 2021, arXiv:2104.03311 [cs]. [Online]. Available: http://arxiv.org/abs/2104.03311

[28] Y. Hu, L. Anderson, T.-M. Li, Q. Sun, N. Carr, J. Ragan-Kelley, and F. Durand, "Difftaichi: Differentiable programming for physical simulation," *ICLR*, 2020.

[29] Z. Zong, C. Jiang, and X. Han, "A Convex Formulation of Frictional Contact for the Material Point Method and Rigid Bodies," in *2024 IEEE/RSJ International Conference on Intelligent Robots and Systems (IROS)*, Oct. 2024, pp. 1831–1838, iSSN: 2153-0866. [Online]. Available: https://ieeexplore.ieee.org/abstract/document/10801598

[30] C. Jiang, C. Schroeder, J. Teran, A. Stomakhin, and A. Selle, "The material point method for simulating continuum materials," in *Acm siggraph 2016 courses*, 2016, pp. 1–52.

[31] D. Metaxas and D. Terzopoulos, "Shape and nonrigid motion estimation through physics-based synthesis," *IEEE Transactions on Pattern Analysis and Machine Intelligence*, vol. 15, no. 6, pp. 580–591, 2002.

[32] A. J. Valencia, F. Nadon, and P. Payeur, "Toward real-time 3d shape tracking of deformable objects for robotic manipulation and shape control," in *2019 IEEE SENSORS*. IEEE, 2019, pp. 1–4.

[33] W. Liu, Y. Song, D. Chen, S. He, Y. Yu, T. Yan, G. P. Hancke, and R. W. Lau, "Deformable object tracking with gated fusion," *IEEE Transactions on Image Processing*, vol. 28, no. 8, pp. 3766–3777, 2019.

[34] J. Xiang, H. Dinkel, H. Zhao, N. Gao, B. Coltin, T. Smith, and T. Bretl, "Trackdlo: Tracking deformable linear objects under occlusion with motion coherence," *IEEE Robotics and Automation Letters*, vol. 8, no. 10, pp. 6179–6186, 2023.

[35] X. Li, Y. Guo, Y. Tu, Y. Ji, Y. Liu, J. Ye, and C. Zheng, "Textureless deformable object tracking with invisible markers," *IEEE Transactions on Pattern Analysis and Machine Intelligence*, vol. 47, no. 9, pp. 7243–7254, 2024.

[36] J. Schulman, A. Lee, J. Ho, and P. Abbeel, "Tracking deformable objects with point clouds," in *2013 IEEE International Conference on Robotics and Automation*. IEEE, 2013, pp. 1130–1137.

[37] Z. Cai, L. Wen, Z. Lei, N. Vasconcelos, and S. Z. Li, "Robust deformable and occluded object tracking with dynamic graph," *IEEE Transactions on Image Processing*, vol. 23, no. 12, pp. 5497–5509, 2014.